iScience

Article

ROS-responsive nanoparticles with selenomethionine for ferroptosis modulation in abdominal aortic aneurysm

Graphical abstract

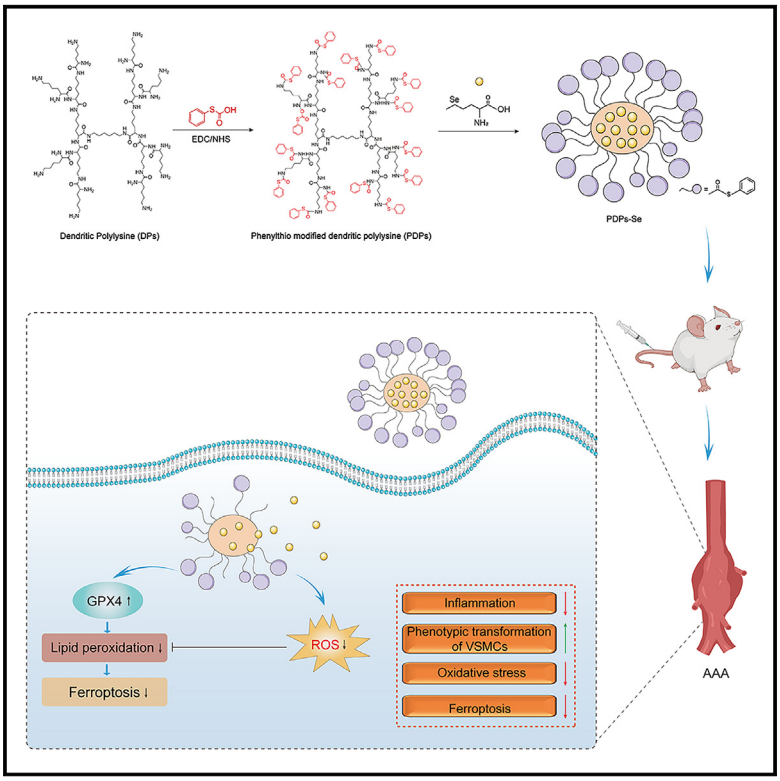

Highlights

- PDPs-Se could enhance ROS scavenging *in vitro* and *in vivo*
- PDPs-Se could target abdominal aortic aneurysm by ROS trigger
- PDPs-Se could attenuate AAA progression by suppressing ferroptosis

Authors

Haipeng He, Lei Chen, Jiaxin Peng, ..., Songbiao Zhan, Xue Han, Weifeng Yao

Correspondence

hanx39@mail.sysu.edu.cn (X.H.), yaowf3@mail.sysu.edu.cn (W.Y.)

In brief

Therapeutics; Nanoparticles; Biological sciences; Bioengineering

He et al., 2025, iScience *28*, 111880
March 21, 2025
https://doi.org/10.1016/j.isci.2025.111880

CellPress

iScience

CellPress
OPEN ACCESS

Article

ROS-responsive nanoparticles with selenomethionine for ferroptosis modulation in abdominal aortic aneurysm

Haipeng He,[1,5] Lei Chen,[2,5] Jiaxin Peng,[1,5] Jinyan Guo,[3] Xue Xiao,[3] Chaoxun Dou,[3] Huining Chen,[1] Songbiao Zhan,[1] Xue Han,[4,6,*] and Weifeng Yao[3,*]

[1]Department of Vascular Surgery, The Third Affiliated Hospital of Sun Yat-Sen University, Guangzhou, China
[2]Department of Vascular Surgery, Zhejiang Provincial People's Hospital, Hangzhou Medical College, Hangzhou, Zhejiang, China
[3]Department of Anesthesia, The Third Affiliated Hospital of Sun Yat-Sen University, Guangzhou, China
[4]Department of Anesthesia, Sun Yat-sen Memorial Hospital of Sun Yat-Sen University, Guangzhou, China
[5]These authors contributed equally
[6]Lead contact
*Correspondence: hanx39@mail.sysu.edu.cn (X.H.), yaowf3@mail.sysu.edu.cn (W.Y.)
https://doi.org/10.1016/j.isci.2025.111880

SUMMARY

Oxidative stress, particularly ROS accumulation, plays a key role in the development of abdominal aortic aneurysm (AAA). Surgical treatments and current drugs for AAA have limitations, including lack of specificity and significant side effects. This study constructed ROS-responsive nanoparticles using phenylthio-modified dendritic polylysine (PDP) loaded with selenomethionine (PDPs-Se) for AAA treatment, and elucidated its mechanism of action. *In-vitro* studies revealed that PDPs-Se enhanced the clearance of ROS by increasing the levels of superoxide dismutase (SOD) and glutathione (GSH) while reducing malondialdehyde (MDA) levels. Furthermore, PDPs-Se upregulated the expression levels of GPX4, SLC7A11, and FTH1 to suppress ferroptosis and modulate the differentiation of vascular smooth muscle cells (VSMCs) from a synthetic to a contractile phenotype. *In-vivo* experiments revealed that PDPs-Se attenuated the progression of AAA by inhibiting oxidative stress responses and improving the aortic wall thickness, indicating its potential as an approach for AAA therapy.

INTRODUCTION

Abdominal aortic aneurysm (AAA) is a common degenerative disease of the aorta characterized by a complex pathogenesis involving chronic inflammation, oxidative stress, and extracellular matrix degradation.[1,2] Treatment options for AAA are limited, with surgical repair being considered only when the aorta diameter dilates sufficiently (greater than 5.5 cm for males or greater than 5.0 cm for females), which indicates high risk of rupture.[3] Once the AAA ruptures, the mortality rate can reach 85%–90%.[4] The incidence and mortality rates of AAA are increasing globally each year, driven in part by an aging population. Currently, the main drugs for AAA prevention and treatment in clinical research include lipid-lowering drugs, antibiotics, antiplatelet drugs, and anti-inflammatory drugs.[5,6] However, the traditional formulations used for these drugs lack targeted delivery to AAA lesions, resulting in unsatisfactory clinical effects and numerous toxic side effects.[7] Therefore, there is an urgent need to develop new strategies for the prevention and treatment of AAA, in addition to innovative targeted drug delivery systems.

Extensive studies have demonstrated that abnormally high levels of reactive oxygen species (ROS) in the abdominal aortic vessel wall are closely associated with the occurrence and progression of AAA inflammation. This involves the recruitment of local inflammatory factors in AAA, phenotypic transformation of vascular smooth muscle cells (VSMCs), generation of matrix metalloproteinases (MMPs), and destruction of the vascular elastic layers, which are considered key pathogenic factors leading to AAA.[8–10] Weintraub et al.[11] reported that the ROS level in the AAA segments of patients' aortic blood vessels is 2.5 times higher than that in non-AAA segments. In an AAA model using apolipoprotein E (ApoE) gene-knockout mice induced by angiotensin II (ANG-II), the ROS level in the abdominal aorta of the disease group was more than 10 times higher than that of the control group.[12] Additionally, a study using a $CaCl_2$-induced AAA rat model reported that the ROS level in the abdominal aorta of the disease group was more than 4 times higher than that of the control group.[13] These findings suggest that antioxidant stress is a highly promising therapeutic strategy. However, methods with strong ROS clearance ability and precise targeting of vascular lesions need to be developed. Recently, ROS-responsive nanotherapies have been reported for targeted treatment of AAA, such as Hu et al.[14] reported a luminol-conjugated α-cyclodextrin nanoparticles for targeting therapy of AAA by site-specifically regulating neutrophilic inflammation, as well as Lin et al.[15] prepared a multi-bioactive nanomicelle for site-specifically

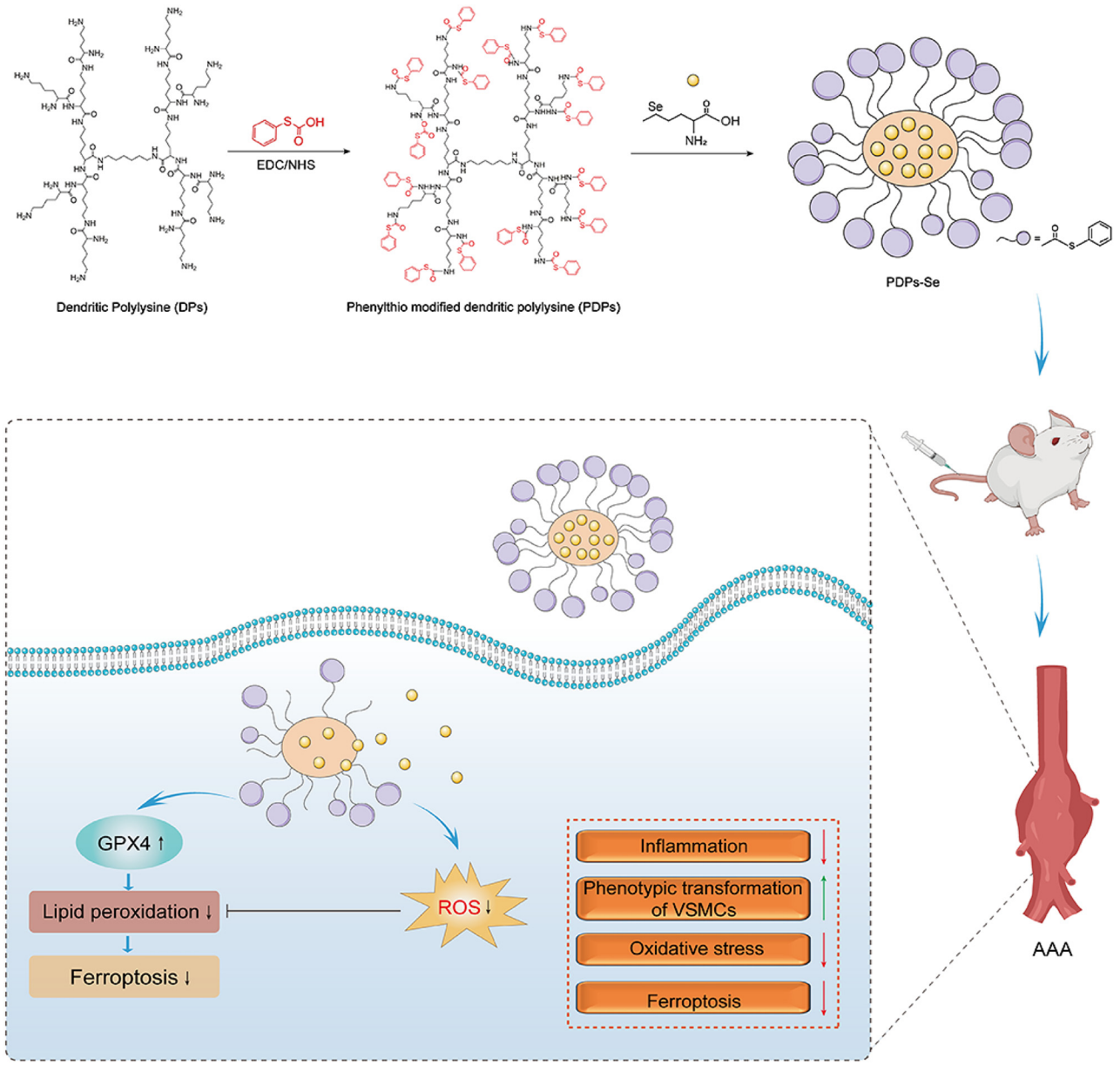

Scheme 1. Schematic illustration of the synthesis of PDPs-Se nanoparticles and their application to AAA treatment

delivering in AAA. Overall, ROS-responsive nanotherapeutic strategies hold greater promise for the treatment of AAA.

Selenium, which is an essential trace elements in the growth process of organisms, is involved in the regulation of various physiological functions in the body and plays important roles in antioxidant stress, cell protection and repair, immune response, detoxification, and cancer prevention, in addition to exhibiting potential anticancer properties.[16,17] Multiple studies have revealed that Se can reduce the expression of reactive oxygen species (ROS) and help fight oxidative stress[18–20] to alleviate disease progression. However, the narrow therapeutic window of selenium between healthy and toxic dosages leads to reduced Se bioavailability, and limiting its clinical application.[21]

Nano drug delivery systems (NDDSs) based on nanomaterials have been extensively investigated.[22,23] Compared with conventional drug administration methods, NDDSs aim to improve the pharmacokinetic properties of drugs, reduce toxicity to normal tissues, and achieve safer and more effective treatment.[24,25] In this study, ROS-responsive PDPs-Se nanoparticles were developed through the self-assembly of benzylthiol-modified hyperbranched polylysine with selenomethionine. PDPs-Se nanoparticles undergo a hydrophobic-hydrophilic transition in the presence of ROS, and release selenomethionine at the target site to exert their antioxidant stress effect, thereby achieving AAA therapy by modulating the ferroptosis and phenotypic transformation of vascular smooth muscle cells (Scheme 1).

RESULTS AND DISCUSSION

Synthesis of ROS-responsive drug release nanoparticles

Phenylthio-modified dendritic polylysine was synthesized using EDC/NHS conjugation chemistry between the -NH2 and -COOH groups (Figure 1A). The successful modification of the phenylthio groups onto dendritic polylysine was confirmed using FIIR spectroscopy. As shown in Figure 1B, the disappearance of the -NH2 peak at approximately 3230 cm-1, along with the appearance of the -S-C=O (at approximately 1130 cm-1) and -Ph (at approximately 680 cm-1) groups in the product spectrum, demonstrates the successful synthesis of PDPs. In addition, chemical structural changes were also confirmed using UV-vis spectroscopy. As shown in Figure 1C, the absorption peaks of PDPs at the wavelengths of 327.6 and 466 nm demonstrate the successful modification of chromophores (-S-C=O and -Ph groups) on the molecule. As the occurrence of substitution reactions, the α-H atoms (a positions) of -NH2 groups of DP disappeared accompanied by the H atoms (b positions) on the benzene rings appeared (Figure S1). From the chemical structures of DP and PDP, the theoretical ratio of the number of hydrogen atoms of a and b position was 3:10. The integral area of a positions and b positions in the spectroscopy were 3.15 and 12.29 (15.71–3.42). Hence we can determine the degree of substitution (DS) of (phenylthio) acetic unit was: DS=(3.15/12.29)/(3/10)*100% = 85.43%. The content of selenomethionine was analyzed by determining the selenium in the selenomethionine-loaded PDP using inductively coupled plasma atomic emission spectroscopy (ICP-AES) at wavelength of 196.26 n. The content of selenomethionine in the nanoparticles was 25.38 mg/g, which was very close to the initial additive amount of 0.3 mg/10 mg (Table S1). As shown in Figure 1D, dendritic polylysine dissolved in water, while PDPs formed a homoturbid solution. The existence of -NH-CO- of the PDPs can form hydrogen bonding interactions with -NH2 and -COOH of the selenomethionine. After being distributed in water, the combination of selenomethionine and PDPs was self-assembly by hydrophobic interaction of the phenylthio groups, formed nanoparticles with structure of selenomethionine as core and PDPs as shell. The introduction of phenylthio end groups led to significant changes in the hydrophilicity of dendritic polylysine. Furthermore, SEM observation was performed to elucidate the microscopic morphology of this turbid solution. The PDPs formed nanoparticles with a diameter of less than 100 nm when dispersed in water, due to its molecular amphiphilicity and the formation of a core-shell structure (Figure 1E). The size dispersion of the nanoparticles was further analyzed using a laser particle size analyzer, and good dispersibility was observed, with more than 85% of the nanoparticles having a diameter of 40–70 nm (Figure 1F). The stability of the nanoparticles, which is related to their zeta potential, was evaluated. As shown in Figure 1G, the zeta potential of dendritic polylysine was −27.9 mV, which is lower than the absolute value of ±30 mV, indicating low stability. However, the zeta potential of PDPs was +46.7 mV, which is higher than the absolute value of ±40 mV, indicating high stability. These results demonstrated that the successful preparation of PDPs-based nanoparticles with good size dispersion and stability. The cumulative release of Se-Met from PDPs-Se in different concentrations of H_2O_2 were examined to monitor the ROS-responsive of PDPs-Se. As shown in Figure S10, PDPs-Se exhibited a higher release in 10 mM H_2O_2 solution compared to 1 mM H_2O_2 solution. This indicates that PDPs-Se could response ROS to release Se-Met.

Biocompatibility of PDPs-Se nanoparticles

Selenium-containing PDPs-Se nanoparticles were synthesized following the procedure outlined in Figure 2A. To assess the biocompatibility of the PDPs-Se nanoparticles, CCK8 was used to detect the cell viability of VSMCs. As shown in Figure S2A, the cell viability of PDPs-Se with different concentrations did not exhibit toxicity under 15 μg/mL. Therefore, we selected a concentration of 15 μg/mL for subsequent experiments. Moreover, Figure 2B showed that exposure to PDPs-Se nanoparticles for 24 h, 48 h, and 72 h did not significantly affect cell viability compared with the control group. Additionally, flow cytometry analysis did not reveal differences in cell apoptosis between the PDPs-Se and control groups, as shown in Figure 2C. These findings suggest that the PDPs-Se nanoparticles are nontoxic to VSMCs. Furthermore, PDPs-Se nanoparticles were intravenously injected into mice and continuously monitored for 7 days. The body weights of the mice did not exhibit any significant changes compared with the control group (Figure 2D). Additionally, blood routine analysis did not identify no significant differences in the red blood cells, white blood cells, platelets, and hemoglobin content between the PDPs-Se and control groups (Figure 2E). The levels of ALT, AST, BUN, and CREA showed that PDPs-Se could not affect the liver and kidney function (Figures S2B–S2E). Moreover, HE staining did not reveal significant pathological alterations in the heart, liver, spleen, lung, and kidney of mice injected with PDPs-Se nanoparticles compared to the control group (Figure 2F). These results indicated that PDPs-Se nanoparticles have excellent biocompatibility.

Inhibition of ROS production and ferroptosis by PDPs-Se

The pathogenesis of AAA is complex, with oxidative stress and the loss of VSMCs playing a key role in its development.[26,27] Growing evidence suggests that ferroptosis is involved in AAA pathogenesis.[28,29] Ferroptosis is an iron-dependent non-apoptotic cell death characterized by the excessive accumulation of lipid peroxides and reactive oxygen species.[30] The occurrence of ferroptosis is associated with the levels of FTH1, SLC7A11, and GPX4, which are key regulators of this process.[31,32] Specifically, FTH1 is a key regulator of iron storage and metabolism during ferroptosis, and affects ferritin deposition and systemic iron metabolism[33]; SLC7A11 is a part of the system Xc-, which regulates intracellular cysteine levels and thus affects GSH synthesis and GPX4 activity[34]; GPX4 is a key molecule in the mechanism of ferroptosis, which relies on Se for bioactivity.[35] Previous studies have shown that the GPX4/GSH antioxidant systems are weakened in AAA, leading to ROS accumulation and the promotion of ferroptosis.[36–38] Additionally, selenomethionine (Se-met) delays the disease progression of osteoarthritis by inhibiting ferroptosis in chondrocytes.[39,40] These findings suggest that inhibiting ferroptosis and delivering Se-Met may be promising therapeutic strategies for AAA.

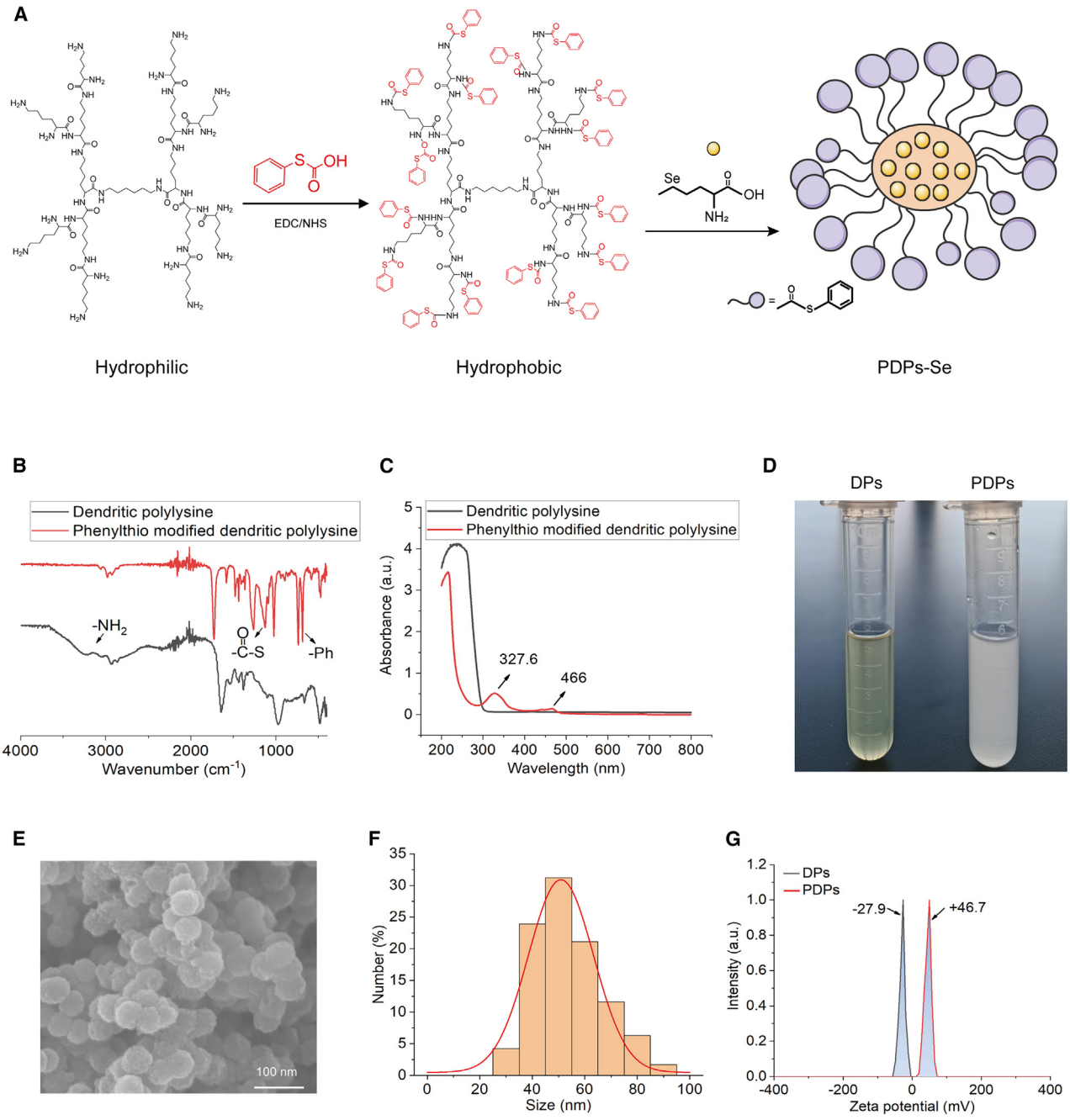

Figure 1. Synthesis and characterization of PDPs and PDPs-Se nanoparticles

(A) Synthesis reaction formula of PDPs-Se.
(B) FTIR spectra of the dendritic polylysine and PDPs.
(C) UV-vis spectra of dendritic polylysine and PDPs.
(D) Photographs of the dendritic polylysine and PDPs dispersed in deionized water.
(E) SEM images of PDPs-Se nanoparticles.
(F) Particle size distribution of PDPs-Se.
(G) Zeta potential of dendritic polylysine and PDPs dispersed in deionized water.

Angiotensin II (ANG-II) was used to induce VSMCs as an AAA model. The endocytosis of PDPs-Se nanoparticles by VSMCs was investigated by immunofluorescence staining. The PDPs-Se were successfully endocytosed into ANG-II-induced VSMCs (Figure S3A). At the same time, we evaluated the *in vivo* targeting of PDPs-Se, Cy7-labeled PDPs-Se were

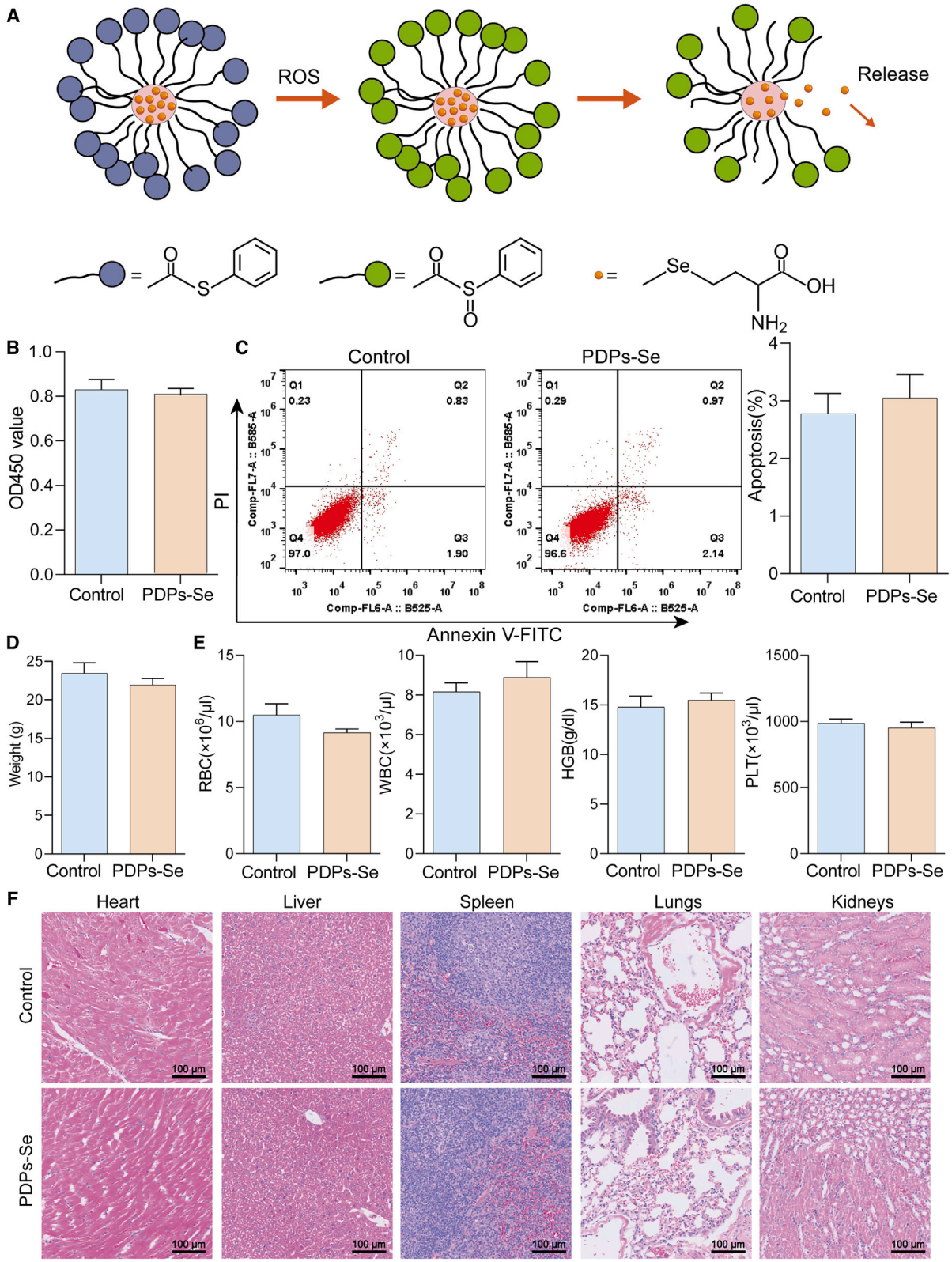

(legend on next page)

intravenously injected via tail vein and allowed to circulate for 24 h. The aortas of the mice *in vivo* and *ex vivo* were imaged using the IVIS imaging system to visualize the signal given by the Cy7-PDPs-Se. As shown in Figure S3B, the region of the mouse aortas aneurysms showed a high fluorescent signal, indicating accumulation of the Cy7-PDPs-Se in the aneurysmal tissue. These results confirmed that PDPs-Se could successfully reach and accumulate in the aneurysmal tissue. Subsequently, CCK8 and Transwell assays were conducted to observe the effects of PDPs-Se nanoparticles on cell viability and migration behavior, and it was found that ANG-II-induced VSMCs cultured on PDPs-Se group possessed higher cell viability and migration ability compared with the PDPs group, indicating that the incorporation of Se could enhance cell viability and promote cell migration (Figures S3C and 3A). It was demonstrated that VSMC could migrate to damaged areas and form new extracellular matrix, thereby enhancing the structural integrity of blood vessels.[41] Consequently, the enhanced migration of VSMCs after PDPs-Se treatment may be a potential protective mechanism contributing to the restoration of the vessel wall and the maintenance of vascular stability. The ROS scavenging ability of PDPs-Se nanoparticles was further evaluated, and found that the PDPs-Se group significantly inhibited the ROS level in VSMCs compared to the control group (Figure S4). Meanwhile, flow cytometry results also indicated that PDPs-Se reduced ROS accumulation in ANG-II-induced VSMCs (Figure 3B). Changes in the SOD, MDA, and GSH levels in ANG-II-induced VSMCs treated with PDPs-Se nanoparticles were assessed by ELISA. The results showed that the SOD and GSH levels in the PDPs-Se group were significantly higher than those in the PDPs group, while the MDA level was significantly lower, indicating that PDPs-Se could significantly improved the oxidative stress response in ANG-II-induced VSMCs (Figure 3C**)**. Notably, we found that the Nrf 2/HO-1 signaling pathway was activated in ANG-II-induced VSMCs and blocked in VSMCs treated with PDPs-Se. Additionally, PDPs-Se significantly downregulated the expression of Nrf 2 and HO-1(Figures S5A and S5B). Next, the level of ferroptosis in VSMCs in the different treatment groups was examined by RT-qPCR. The results revealed that the mRNA levels of GPX4, FTH1, and SLC7A11 in the PDPs-Se group were significantly higher than those in the PDPs and ANG-II groups (Figure S6). Furthermore, immunofluorescence detection of GPX4 expression confirmed that the PDPs-Se group exhibited significantly higher GPX4 expression compared with the PDPs and ANG-II groups (Figure 3D). Meanwhile, western blotting analysis indicated that the protein levels of FTH1 and SLC7A11 in the PDPs-Se group were significantly increased compared to the ANG-II and PDPs groups (Figure 3E). These results demonstrated that the PDPs-Se nanoparticles could significantly inhibit ferroptosis in VSMCs.

Inhibition of inflammation and metabolic imbalance by PDPs-Se

Ferroptosis is closely associated with the inflammatory responses, wherein cells undergoing ferroptosis release specific cytokines to promote inflammation-related reactions.[40] Studies have shown that the inhibition of ferroptosis significantly alleviates conditions, such as non-alcoholic fatty liver disease, neuroinflammation, and metabolic inflammation.[42,43] In AAA, VSMCs in the aneurysmal wall accumulate ROS due to ferroptosis, triggering the release of many inflammatory factors, enhanced synthesis of matrix metalloproteinases, and accelerated degradation of the vascular wall, in addition to promote the progression of AAA.[37] Therefore, the inhibition of ferroptosis may be a crucial pathway toward alleviating AAA. To investigate whether PDPs-Se nanoparticles can inhibit the inflammatory response in AAA, VSMCs were induced *in vitro* using ANG-II. The results found that treatment with PDPs-Se nanoparticles significantly downregulated the mRNA levels of TNF-α, IL-6, and IL-1β compared to the PDPs group and ANG-II group (Figure S7A). Western blot results also supported these findings (Figure S7B), indicating that PDPs-Se nanoparticles effectively improved the inflammatory response in AAA. Moreover, previous studies have found that an extracellular matrix (ECM) metabolic imbalance in the arterial wall plays a key role in the progression of AAA.[44] Therefore, the expression levels of MMP2 and MMP9 genes were evaluated using RT-qPCR. The results showed that the PDPs-Se group had significantly lower mRNA levels of MMP2 and MMP9 compared to the PDPs and ANG-II groups (Figure 4A). Similarly, the protein levels of MMP2 and MMP9 in the PDPs-Se group were lower than those in the other groups (Figure 4B), indicating that PDPs-Se nanoparticles restored the ECM imbalance in the arterial wall.

In the abdominal aorta, VSMCs are mainly located in the medial layer of the artery and play a crucial role in regulating vascular tension, blood pressure, and blood flow through their contraction and dilation abilities. The dysfunction of VSMCs is a key pathological feature of AAA, and is associated with AAA expansion and rupture.[45] Research has found that impaired contractile ability of smooth muscle cells in patients with AAA, characterized by the downregulation of differentiation markers, such as the smooth muscle actin and smooth muscle myosin heavy chain. This indicates a transition from a differentiated contractile phenotype to a dedifferentiated synthetic phenotype.[46] To further explore the impact of PDPs-Se nanoparticles on the phenotypic transition of VSMCs, the expression levels of OPN and α-SMA genes were evaluated by RT-qPCR. The results showed that the mRNA level of OPN in the PDPs-Se group was significantly lower than in the other groups, while the opposite is true for α-SMA (Figure 4C). Immunofluorescence also showed the same results (Figure 4D), indicating that PDPs-Se

Figure 2. Biocompatibility of the PDPs-Se nanoparticles

(A) Schematic illustration of encapsulation of selenocysteine in Se-containing nanoparticles.

(B) Cell viability of VSMCs was assessed using the CCK8 assay.

(C) Analysis of VSMCs apoptosis by flow cytometry.

(D) Mouse weight measured using an electronic balance.

(E) Detection of blood routine with a blood cell analyzer.

(F) Evaluation of condition of mouse heart, liver, spleen, lung, and kidney through HE staining (scale bar: 100 μm). (n = 3).

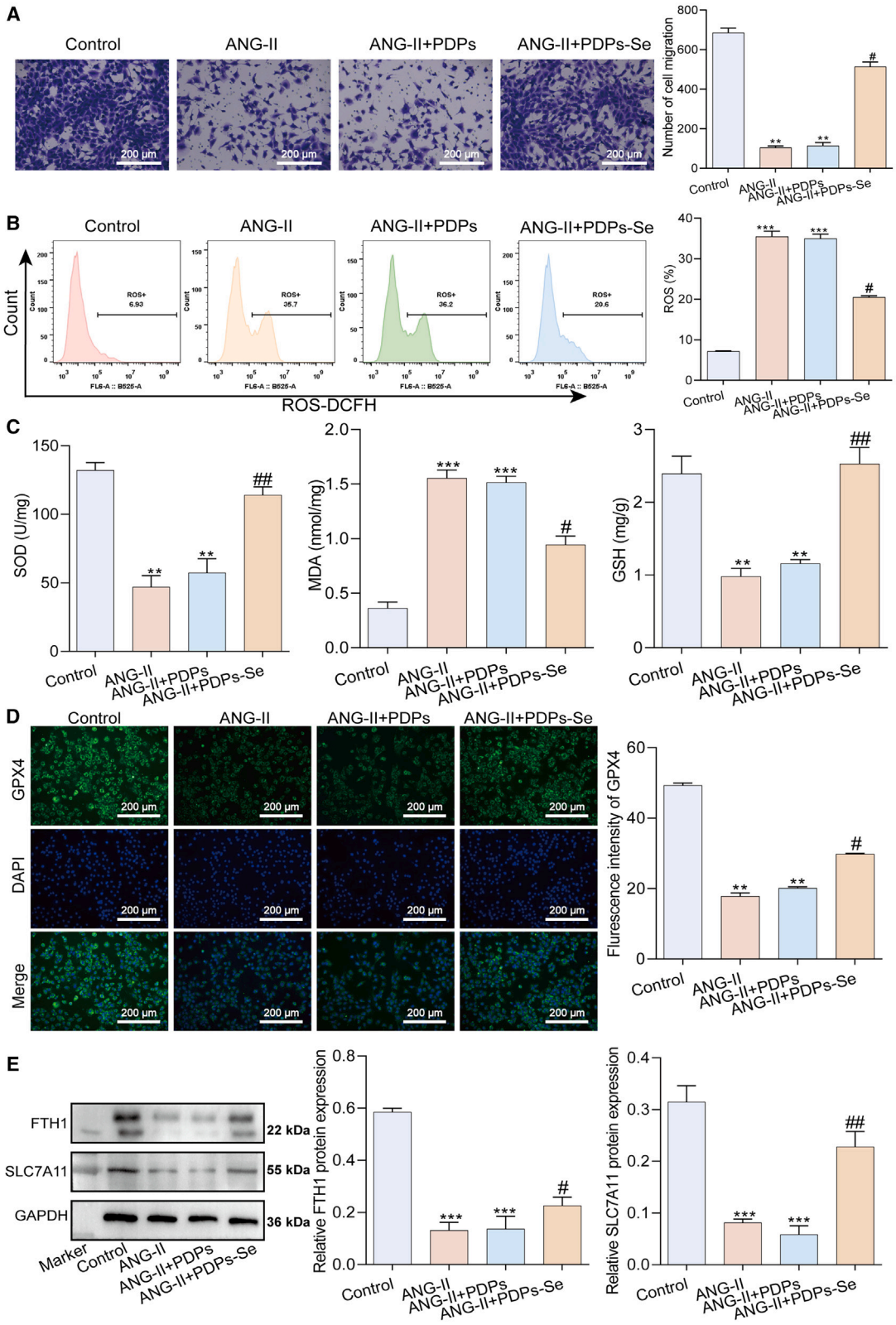

(legend on next page)

could promote the transition of VSMCs from the synthetic phenotype to the contractile phenotype, thereby improving the progress of AAA.

Inhibition of AAA procession *in vivo* by PDPs-Se

To evaluate the therapeutic effect of PDPs-Se nanoparticles *in vivo*, abdominal aortas from different groups of treated mice were collected and examined for damage to the abdominal aortas using HE staining. The results showed that the abdominal aortic wall thickness and diameter in the PDPs-Se group was significantly smaller than that in the PDPs and model groups (Figure 5A), with a notable reduction in collagen deposition (Figure 5B). Moreover, similar results also showed in Victoria blue staining (Figure S9). The apoptosis levels of VSMCs in the PDPs and model groups were significantly higher than those in the sham-operated group. However, this trend is reversed in PDPs-Se group, where PDPs-Se treatment inhibited VSMCs apoptosis (Figure 5C). Furthermore, the levels of inflammatory factors in the mouse serum were analyzed via ELISA. As shown in Figure S8, the contents of TNF-α, IL-6, and IL-1β in the PDPs-Se group were significantly lower than those in the PDPs and model groups. Collectively, these results collectively indicate that the PDPs-Se nanoparticles exhibited a good therapeutic effect on AAA *in vivo*.

Inhibition of ferroptosis in mice of AAA by PDPs-Se

To assess the impact of PDPs-Se nanoparticles on ferroptosis in AAA, this study assessed the oxidative stress response in mice, and the expression levels of SOD, MDA, and GSH proteins were measured by ELISA. Compared with the model group, the SOD and GSH levels were significantly upregulated, whereas MDA was notably decreased in the PDPs-Se group (Figure 6A). Additionally, the mRNA levels of GPX4, FTH1, and SLC7A11 in the PDPs-Se group were firstly analyzed by RT-qPCR. As shown in Figure 6B, the expression levels of GPX4, FTH1, and SLC7A11 genes were significantly higher than those in the PDPs and model groups. Furthermore, immunofluorescence staining results revealed that the expression level of GPX4 protein in the PDPs-Se group was significantly higher compared to that in the PDPs and model groups (Figure 6C). Additionally, the protein levels of SLC7A11 and FTH1 (Figure 6D) were notably elevated. These findings indicate that PDPs-Se could significantly inhibit ferroptosis in mice with AAA.

Reversal of phenotypic transformation in AAA mice by PDPs-Se

MMP2 and MMP9 are important members of the MMP family and play key roles in extracellular matrix hydrolysis and vascular wall integrity.[47,48] Therefore, the expression levels of MMP2 and MMP9 genes in the abdominal aorta of mice in different groups were further analyzed by RT-qPCR. As shown in Figure 7A, the mRNA levels of MMP2 and MMP9 were significantly higher in the PDPs-Se group compared with the PDPs and model groups. The same results obtained by western blot (Figure 7B), indicating that PDPs-Se nanoparticles could significantly improved the activity of matrix metalloproteinases and alleviated vascular wall damage. Notably, VSMCs undergo phenotypic transformation during aneurysm development, with a shift from a contractile to a proliferative phenotype.[49,50] This transformation leads to a decrease in contractile smooth muscle cells marked by α-SMA expression, and an increase in synthetic smooth muscle cells marked by OPN, thereby increasing the risk of aneurysm rupture.[6] The expression levels of α-SMA and OPN proteins were further detected by western blot. The results revealed that the expression level of α-SMA in the PDPs-Se group was significantly higher than that in the PDPs and model groups, while opposite is the case for the expression of OPN (Figure 7C). This indicates that PDPs-Se nanoparticles reversed the phenotypic transformation of AAA *in vivo*.

This study used benzylthiol-modified hyperbranched polylysines to construct amphiphilic molecules responsive to ROS. These molecules successfully self-assembled with selenomethionine to form ROS-responsive PDPs-Se nanoparticles with good size dispersion and stability. The PDPs-Se nanoparticles exhibited biocompatibility because they were nontoxic to VSMCs and did not induce organ pathology upon intravenous administration *in vivo*. *In-vitro* cells experiments showed that the ROS-responsive PDPs-Se nanoparticles could effectively suppress ferroptosis, attenuated inflammatory responses, and facilitate the transition of VSMCs from a synthetic to a contractile phenotype. Furthermore, *in-vivo* experiments in mice with AAA demonstrated that PDPs-Se nanoparticles exerted a good therapeutic effect by inhibiting inflammation, oxidative stress and ferroptosis, as well as reversing the phenotypic transformation of VSMCs, suggesting a promising targeted treatment strategy for AAA.

Limitations of the study

Though the therapeutic effect of PDPs-Se was verified *in vitro* and *in vivo* experiments, their pharmacokinetics is still unclear. Additionally, while the focus was on oxidative stress and ferroptosis, the deeper mechanisms of the therapeutic effect in AAA progression were not explored.

RESOURCE AVAILABILITY

Lead contact

Further information and requests for resources and reagents should be directed to and will be fulfilled by the lead contact, Xue Han (hanx39@mail.sysu.edu.cn).

Figure 3. PDPs-Se inhibited ferroptosis in ANG-II-induced VSMCs

(A) The migration ability of the VSMCs was examined by Transwell experiment (scale bar: 200 μm).

(B) Flow cytometry was used to evaluate the levels of ROS in VSMCs.

(C) ELISA was used to evaluate the levels of SOD, MDA, and GSH in VSMCs.

(D) Immunofluorescence analysis of GPX4 in VSMCs (scale bar: 200 μm).

(E) Western blotting was conducted to detect the protein levels of FTH1 and SLC7A11 in VSMCs. $n = 3$, data are represented as mean ± SD. t test was utilized for statistical analysis. $^{**}p < 0.01$, $^{***}p < 0.001$ vs. Control group, $\#p < 0.05$, $\#\#p < 0.01$vs ANG-II+PDPs group.

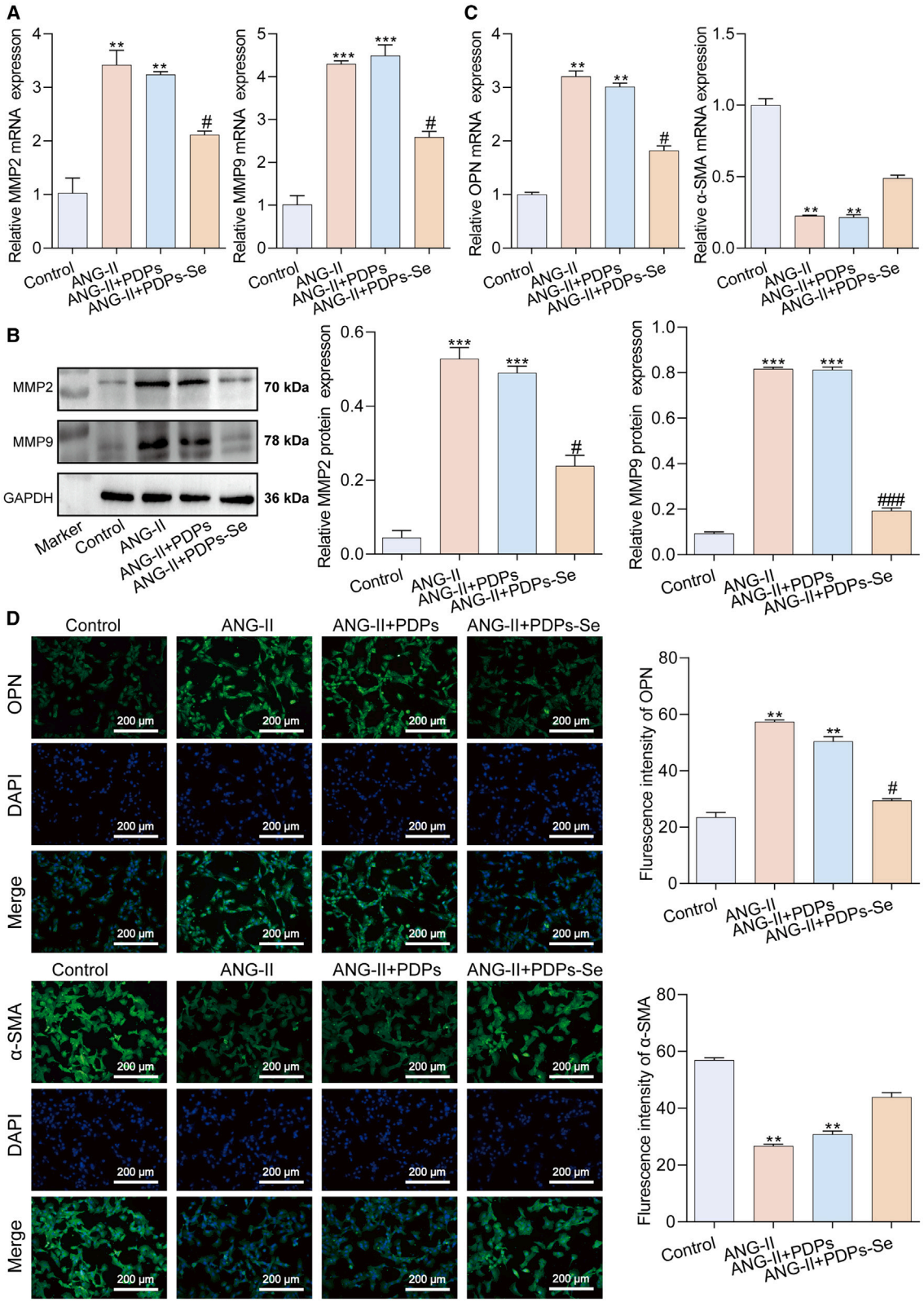

(legend on next page)

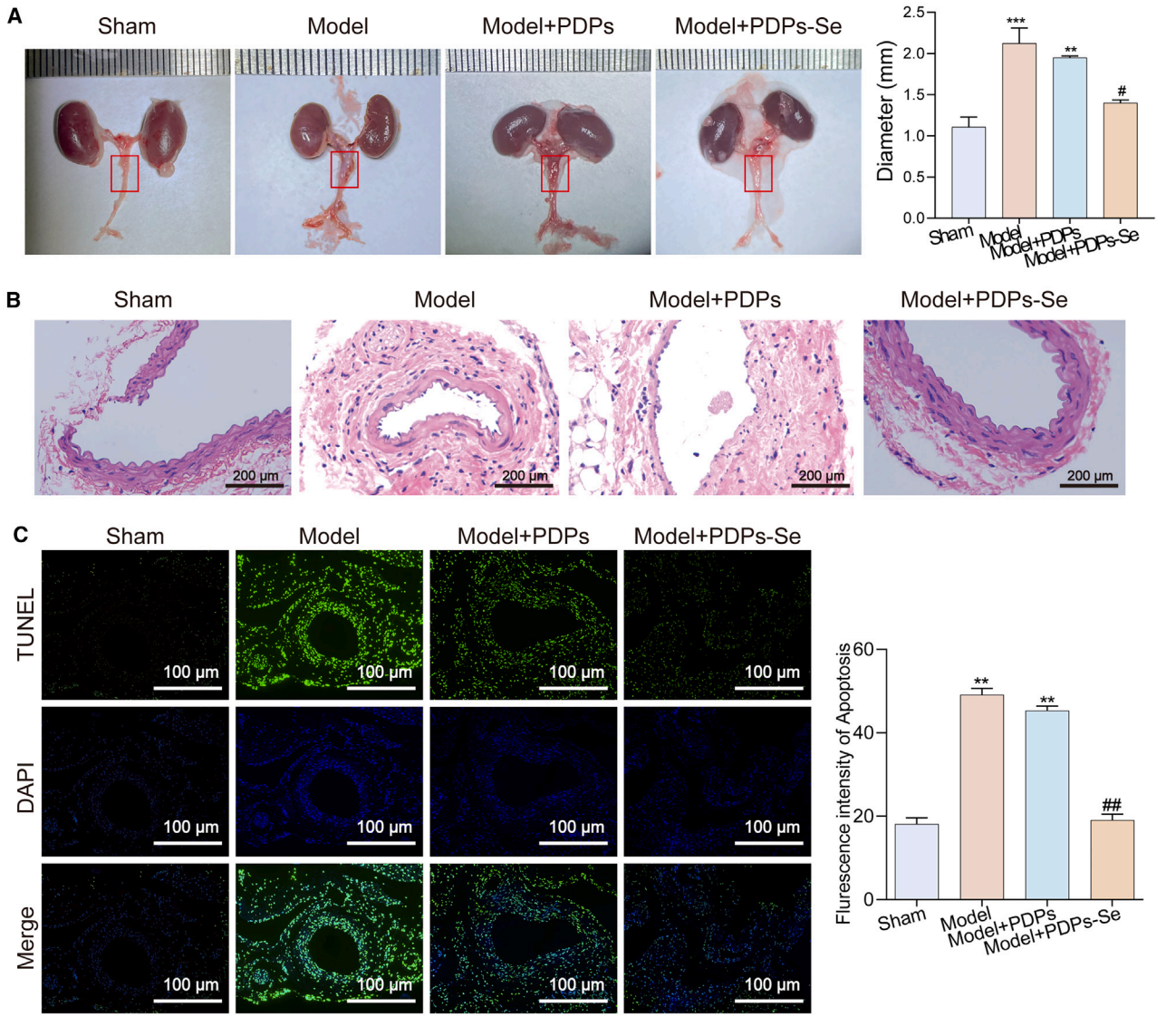

Figure 5. Inhibition of AAA procession in vivo by PDPs-Se

(A) Photographs and diameter of abdominal aortas collected from different groups of treated mice.

(B) HE staining of the abdominal aorta (scale bar: 200 μm).

(C) TUNEL staining estimated the apoptosis levels of VSMCs (scale bar: 100 μm). $n = 3$, data are represented as mean ± SD. t test was utilized for statistical analysis. $^{**}p < 0.01$ vs. sham group, $\#\#p < 0.01$ vs. Model+PDPs group.

Materials availability

This study did not generate new unique reagents or cell lines.

Data and code availability

- All data supporting the findings of this study are found within the article and its supplemental information.
- This article does not report the original code.
- Any additional information about the data reported in this paper will be shared by the lead contact upon request.

ACKNOWLEDGMENTS

This work was financially supported by the National Natural Science Foundation of China (81974081), Natural Science Foundation of China (No. 81900578), the

Figure 4. Inhibition of metabolic imbalance in ANG-II-induced VSMCs by PDPs-Se

(A) The mRNA levels of MMP2 and MMP9 in VSMCs detected by RT-qPCR.

(B) Protein levels of MMP2 and MMP9 in VSMCs detected by western blot.

(C) The mRNA levels of OPN and α-SMA in VSMCs detected by RT-qPCR.

(D) Immunofluorescence staining for OPN and α-SMA proteins in VSMCs (scale bar: 200 μm). $n = 3$, data are represented as mean ± SD. t test was utilized for statistical analysis. $^{**}p < 0.01$, $^{***}p < 0.001$ vs. Control group, $\#p < 0.05$, $\#\#\#p < 0.001$vs ANG-II+PDPs group.

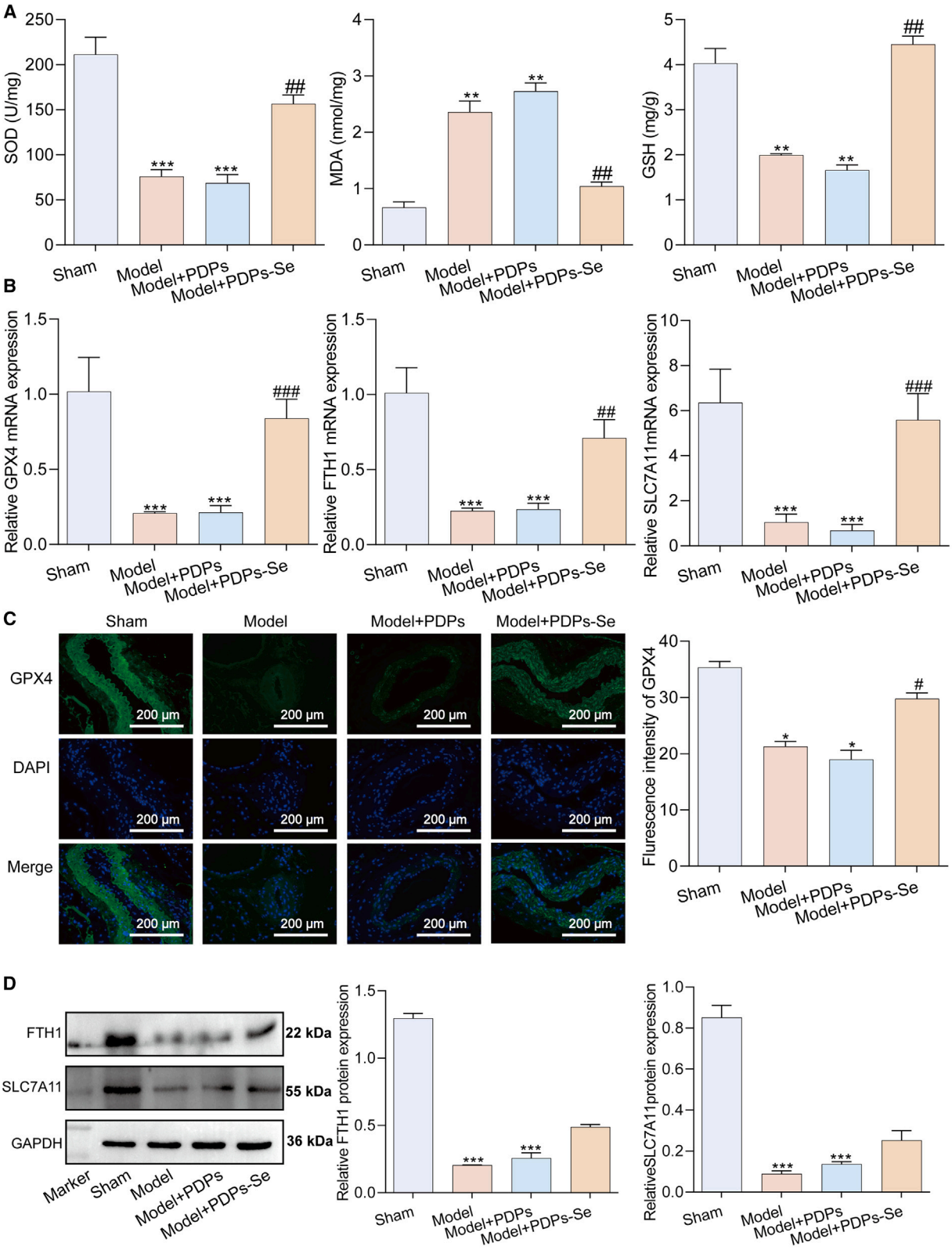

(legend on next page)

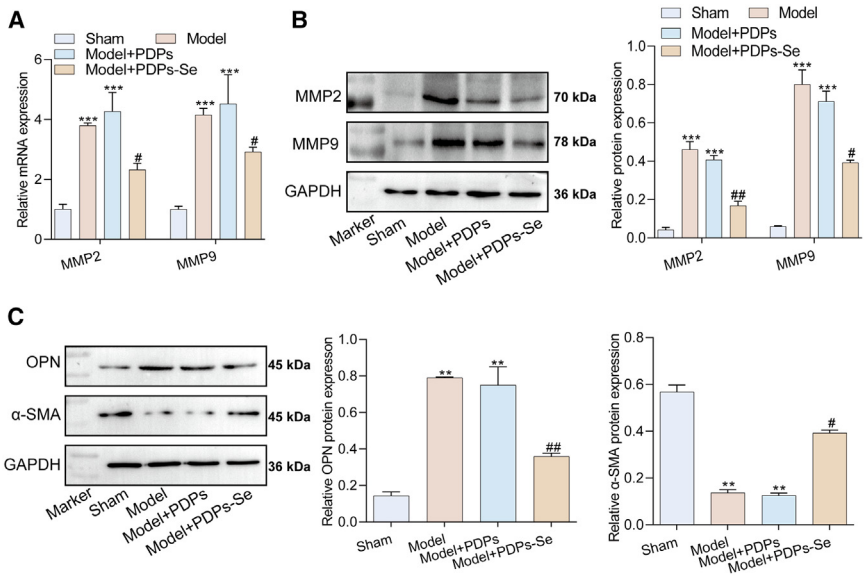

Figure 7. Reversal of phenotypic transformation of AAA mice by PDPs-Se

(A) The mRNA levels of MMP2 and MMP9 in aneurysm tissues detected by RT-qPCR.

(B) Protein levels of MMP2 and MMP9 in aneurysm tissue detected by western blot.

(C) The expression levels of OPN and α-SMA in aneurysm tissues detected by western blot. $n = 3$, data are represented as mean ± SD. t test was utilized for statistical analysis. $^{**}p < 0.01$, $^{***}p < 0.001$ vs. sham group, $\#p < 0.05$, $\#\#p < 0.01$ vs. Model+PDPs group.

Science and Technology Program of Guangzhou (No. 202201020261), the Guangdong Basic and Applied Basic Research Foundation (No. 2019A1515011101) and Guangzhou Science and the Science and Technology Program of Guangzhou (No. 2025A03J3190).

AUTHOR CONTRIBUTIONS

Conceptualization, H.H., L.C., and J.P.; investigation, H.H., L.C., J.P., J.G., X.X., C.D., H.C., and S.Z.; data curation, H.H., L.C., J.P., X.H., and W.Y.; writing—original draft, H.H., L.C., and J.P.; writing—review and editing, all authors; visualization, J.G., X.X., C.D., H.C., and S.Z.; supervision, X.H. and W.Y.

DECLARATION OF INTERESTS

The authors declare that they have no competing interests.

STAR★METHODS

Detailed methods are provided in the online version of this paper and include the following:

SUPPLEMENTAL INFORMATION

Supplemental information can be found online at https://doi.org/10.1016/j.isci.2025.111880.

Received: September 3, 2024
Revised: December 2, 2024
Accepted: January 21, 2025
Published: January 23, 2025

REFERENCES

1. Emeto, T.I., Moxon, J.V., Au, M., and Golledge, J. (2016). Oxidative stress and abdominal aortic aneurysm: potential treatment targets. Clin. Sci. *130*, 301–315. https://doi.org/10.1042/cs20150547.
2. Sulistyowati, E., Huang, S.E., Cheng, T.L., Chao, Y.Y., Li, C.Y., Chang, C.W., Lin, M.X., Lin, M.C., and Yeh, J.L. (2023). Vasculoprotective Potential of Baicalein in Angiotensin II-Infused Abdominal Aortic Aneurysms through Inhibiting Inflammation and Oxidative Stress. Int. J. Mol. Sci. *24*, 16004. https://doi.org/10.3390/ijms242116004.
3. Dyall-Smith, D. (1996). Alopecia areata in a renal transplant recipient on cyclosporin. Australas. J. Dermatol. *37*, 226–227. https://doi.org/10.1111/j.1440-0960.1996.tb01066.x.
4. Gentille-Lorente, D.I., and Salvadó-Usach, T. (2011). [Screening for abdominal aortic aneurysm by means of transthoracic echocardiography]. Rev. Esp. Cardiol. *64*, 395–400. https://doi.org/10.1016/j.recesp.2010.11.009.

Figure 6. Inhibition of ferroptosis in AAA mice by PDPs-Se

(A) The levels of SOD, MDA, and GSH in VSMCs detected by ELISA.

(B) The mRNA levels of GPX4, FTH1, and SLC7A11 in aneurysm tissue detected by RT-qPCR.

(C) Immunofluorescence staining of GPX4 in aneurysm tissue.

(D) Protein levels of FTH1 and SLC7A11 in aneurysm tissue detected by western blot. $n = 3$, data are represented as mean ± SD. t test was utilized for statistical analysis. $^{*}p < 0.05$, $^{**}p < 0.01$, $^{***}p < 0.01$ vs. sham group, $\#p < 0.05$, $\#\#p < 0.01$, $\#\#\#p < 0.001$ vs. Model+PDPs group.

5. Golledge, J., Moxon, J.V., Singh, T.P., Bown, M.J., Mani, K., and Wanhainen, A. (2020). Lack of an effective drug therapy for abdominal aortic aneurysm. J. Intern. Med. *288*, 6–22. https://doi.org/10.1111/joim.12958.

6. Duan, L., Li, S., Wang, L., Jing, Y., Li, G., Sun, Y., Sun, W., Li, Y., Zhao, L., and Xin, S. (2020). Melatonin Plays a Critical Protective Role in Nicotine-Related Abdominal Aortic Aneurysm. Front. Physiol. *11*, 866. https://doi.org/10.3389/fphys.2020.00866.

7. Lederle, F.A. (2013). Abdominal aortic aneurysm: still no pill. Ann. Intern. Med. *159*, 852–853. https://doi.org/10.7326/0003-4819-159-12-201312170-00012.

8. Zhang, Y., Murugesan, P., Huang, K., and Cai, H. (2020). NADPH oxidases and oxidase crosstalk in cardiovascular diseases: novel therapeutic targets. Nat. Rev. Cardiol. *17*, 170–194. https://doi.org/10.1038/s41569-019-0260-8.

9. McCormick, M.L., Gavrila, D., and Weintraub, N.L. (2007). Role of oxidative stress in the pathogenesis of abdominal aortic aneurysms. Arterioscler. Thromb. Vasc. Biol. *27*, 461–469. https://doi.org/10.1161/01.Atv.0000257552.94483.14.

10. Nosoudi, N., Chowdhury, A., Siclari, S., Parasaram, V., Karamched, S., and Vyavahare, N. (2016). Systemic Delivery of Nanoparticles Loaded with Pentagalloyl Glucose Protects Elastic Lamina and Prevents Abdominal Aortic Aneurysm in Rats. J. Cardiovasc. Transl. Res. *9*, 445–455. https://doi.org/10.1007/s12265-016-9709-x.

11. Miller, F.J., Jr., Sharp, W.J., Fang, X., Oberley, L.W., Oberley, T.D., and Weintraub, N.L. (2002). Oxidative stress in human abdominal aortic aneurysms: a potential mediator of aneurysmal remodeling. Arterioscler. Thromb. Vasc. Biol. *22*, 560–565. https://doi.org/10.1161/01.atv.0000013778.72404.30.

12. Thomas, M., Gavrila, D., McCormick, M.L., Miller, F.J., Jr., Daugherty, A., Cassis, L.A., Dellsperger, K.C., and Weintraub, N.L. (2006). Deletion of p47phox attenuates angiotensin II-induced abdominal aortic aneurysm formation in apolipoprotein E-deficient mice. Circulation *114*, 404–413. https://doi.org/10.1161/circulationaha.105.607168.

13. Cheng, J., Zhang, R., Li, C., Tao, H., Dou, Y., Wang, Y., Hu, H., and Zhang, J. (2018). A Targeting Nanotherapy for Abdominal Aortic Aneurysms. J. Am. Coll. Cardiol. *72*, 2591–2605. https://doi.org/10.1016/j.jacc.2018.08.2188.

14. Hu, K., Zhong, L., Lin, W., Zhao, G., Pu, W., Feng, Z., Zhou, M., Ding, J., and Zhang, J. (2024). Pathogenesis-Guided Rational Engineering of Nanotherapies for the Targeted Treatment of Abdominal Aortic Aneurysm by Inhibiting Neutrophilic Inflammation. ACS Nano *18*, 6650–6672. https://doi.org/10.1021/acsnano.4c00120.

15. Lin, W., Hu, K., Li, C., Pu, W., Yan, X., Chen, H., Hu, H., Deng, H., and Zhang, J. (2022). A Multi-Bioactive Nanomicelle-Based "One Stone for Multiple Birds" Strategy for Precision Therapy of Abdominal Aortic Aneurysms. Adv. Mater. *34*, e2204455. https://doi.org/10.1002/adma.202204455.

16. Pang, K.L., and Chin, K.Y. (2019). Emerging Anticancer Potentials of Selenium on Osteosarcoma. Int. J. Mol. Sci. *20*, 5318. https://doi.org/10.3390/ijms20215318.

17. Huang, Q., Liu, Z., Yang, Y., Yang, Y., Huang, T., Hong, Y., Zhang, J., Chen, Q., Zhao, T., Xiao, Z., et al. (2023). Selenium Nanodots (SENDs) as Antioxidants and Antioxidant-Prodrugs to Rescue Islet β Cells in Type 2 Diabetes Mellitus by Restoring Mitophagy and Alleviating Endoplasmic Reticulum Stress. Adv. Sci. *10*, e2300880. https://doi.org/10.1002/advs.202300880.

18. Gong, G., Méplan, C., Gautrey, H., Hall, J., and Hesketh, J.E. (2012). Differential effects of selenium and knock-down of glutathione peroxidases on TNFα and flagellin inflammatory responses in gut epithelial cells. Genes Nutr. *7*, 167–178. https://doi.org/10.1007/s12263-011-0256-4.

19. Hassanin, K.M.A., Abd El-Kawi, S.H., and Hashem, K.S. (2013). The prospective protective effect of selenium nanoparticles against chromium-induced oxidative and cellular damage in rat thyroid. Int. J. Nanomed. *8*, 1713–1720. https://doi.org/10.2147/ijn.S42736.

20. Wu, Z.L., Yin, X.B., Lin, Z.Q., Bañuelos, G.S., Yuan, L.X., Liu, Y., and Li, M. (2014). Inhibitory effect of selenium against Penicillium expansum and its possible mechanisms of action. Curr. Microbiol. *69*, 192–201. https://doi.org/10.1007/s00284-014-0573-0.

21. Zhang, J., Wang, X., and Xu, T. (2008). Elemental selenium at nano size (Nano-Se) as a potential chemopreventive agent with reduced risk of selenium toxicity: comparison with se-methylselenocysteine in mice. Toxicol. Sci. *101*, 22–31. https://doi.org/10.1093/toxsci/kfm221.

22. Huang, D., and Wu, D. (2018). Biodegradable dendrimers for drug delivery. Mater. Sci. Eng. C Mater. Biol. Appl. *90*, 713–727. https://doi.org/10.1016/j.msec.2018.03.002.

23. Zhang, H., Dong, S., Li, Z., Feng, X., Xu, W., Tulinao, C.M.S., Jiang, Y., and Ding, J. (2020). Biointerface engineering nanoplatforms for cancer-targeted drug delivery. Asian J. Pharm. Sci. *15*, 397–415. https://doi.org/10.1016/j.ajps.2019.11.004.

24. Arranja, A.G., Pathak, V., Lammers, T., and Shi, Y. (2017). Tumor-targeted nanomedicines for cancer theranostics. Pharmacol. Res. *115*, 87–95. https://doi.org/10.1016/j.phrs.2016.11.014.

25. Najahi-Missaoui, W., Arnold, R.D., and Cummings, B.S. (2020). Safe Nanoparticles: Are We There Yet? Int. J. Mol. Sci. *22*, 385. https://doi.org/10.3390/ijms22010385.

26. Geng, N., Chen, T., Chen, L., Zhang, H., Sun, L., Lyu, Y., Che, X., Xiao, Q., Tao, Z., and Shao, Q. (2022). Nuclear receptor Nur77 protects against oxidative stress by maintaining mitochondrial homeostasis via regulating mitochondrial fission and mitophagy in smooth muscle cell. J. Mol. Cell. Cardiol. *170*, 22–33. https://doi.org/10.1016/j.yjmcc.2022.05.007.

27. Xie, J., Tang, Z., Chen, Q., Jia, X., Li, C., Jin, M., Wei, G., Zheng, H., Li, X., Chen, Y., et al. (2023). Clearance of Stress-Induced Premature Senescent Cells Alleviates the Formation of Abdominal Aortic Aneurysms. Aging Dis. *14*, 1778–1798. https://doi.org/10.14336/ad.2023.0215.

28. Zhuang, J., Zhu, H., Cheng, Z., Hu, X., Yu, X., Li, J., Liu, H., Tang, P., Zhang, Y., Xiong, X., and Deng, H. (2023). PCSK9, a novel immune and ferroptosis related gene in abdominal aortic aneurysm neck. Sci. Rep. *13*, 6054. https://doi.org/10.1038/s41598-023-33287-9.

29. Wu, H., Chen, L., Lu, K., Liu, Y., Lu, W., Jiang, J., and Weng, C. (2023). HMGB2 Deficiency Mitigates Abdominal Aortic Aneurysm by Suppressing Ang-II-Caused Ferroptosis and Inflammation via NF-κβ Pathway. Mediat. Inflamm. *2023*, 2157355. https://doi.org/10.1155/2023/2157355.

30. Lei, G., Mao, C., Yan, Y., Zhuang, L., and Gan, B. (2021). Ferroptosis, radiotherapy, and combination therapeutic strategies. Protein Cell *12*, 836–857. https://doi.org/10.1007/s13238-021-00841-y.

31. Wang, L., Liu, Y., Du, T., Yang, H., Lei, L., Guo, M., Ding, H.F., Zhang, J., Wang, H., Chen, X., and Yan, C. (2020). ATF3 promotes erastin-induced ferroptosis by suppressing system Xc. Cell Death Differ. *27*, 662–675. https://doi.org/10.1038/s41418-019-0380-z.

32. Hu, X., He, Y., Han, Z., Liu, W., Liu, D., Zhang, X., Chen, L., Qi, L., Chen, L., Luo, Y., et al. (2022). PNO1 inhibits autophagy-mediated ferroptosis by GSH metabolic reprogramming in hepatocellular carcinoma. Cell Death Dis. *13*, 1010. https://doi.org/10.1038/s41419-022-05448-7.

33. Fang, Y., Chen, X., Tan, Q., Zhou, H., Xu, J., and Gu, Q. (2021). Inhibiting Ferroptosis through Disrupting the NCOA4-FTH1 Interaction: A New Mechanism of Action. ACS Cent. Sci. *7*, 980–989. https://doi.org/10.1021/acscentsci.0c01592.

34. Koppula, P., Zhuang, L., and Gan, B. (2021). Cystine transporter SLC7A11/xCT in cancer: ferroptosis, nutrient dependency, and cancer therapy. Protein Cell *12*, 599–620. https://doi.org/10.1007/s13238-020-00789-5.

35. Alim, I., Caulfield, J.T., Chen, Y., Swarup, V., Geschwind, D.H., Ivanova, E., Seravalli, J., Ai, Y., Sansing, L.H., Ste Marie, E.J., et al. (2019). Selenium Drives a Transcriptional Adaptive Program to Block Ferroptosis and Treat Stroke. Cell *177*, 1262–1279.e25. https://doi.org/10.1016/j.cell.2019.03.032.

36. Rochette, L., Dogon, G., Rigal, E., Zeller, M., Cottin, Y., and Vergely, C. (2022). Lipid Peroxidation and Iron Metabolism: Two Corner Stones in

the Homeostasis Control of Ferroptosis. Int. J. Mol. Sci. *24*, 449. https://doi.org/10.3390/ijms24010449.

37. He, X., Xiong, Y., Liu, Y., Li, Y., Zhou, H., and Wu, K. (2024). Ferrostatin-1 inhibits ferroptosis of vascular smooth muscle cells and alleviates abdominal aortic aneurysm formation through activating the SLC7A11/GPX4 axis. Faseb j *38*, e23401. https://doi.org/10.1096/fj.202300198RRR.
38. Ingold, I., Berndt, C., Schmitt, S., Doll, S., Poschmann, G., Buday, K., Roveri, A., Peng, X., Porto Freitas, F., Seibt, T., et al. (2018). Selenium Utilization by GPX4 Is Required to Prevent Hydroperoxide-Induced Ferroptosis. Cell *172*, 409–422.e21. https://doi.org/10.1016/j.cell.2017.11.048.
39. Yu, H., Song, Z., Yu, J., Ren, B., Dong, Y., You, Y., Zhang, Z., Jia, C., Zhao, Y., Zhou, X., et al. (2024). Supramolecular self-assembly of EGCG-selenomethionine nanodrug for treating osteoarthritis. Bioact. Mater. *32*, 164–176. https://doi.org/10.1016/j.bioactmat.2023.09.020.
40. Kiełczykowska, M., Kocot, J., Paździor, M., and Musik, I. (2018). Selenium - a fascinating antioxidant of protective properties. Adv. Clin. Exp. Med. *27*, 245–255. https://doi.org/10.17219/acem/67222.
41. Xue, M., Li, D., Wang, Z., Mi, L., Cao, S., Zhang, L., and Kong, X. (2021). IFI16 contributes to the pathogenesis of abdominal aortic aneurysm by regulating the caspase-1/IL-1β/MCPIP1 pathway. Life Sci. *265*, 118752. https://doi.org/10.1016/j.lfs.2020.118752.
42. Wang, C., Chen, S., Guo, H., Jiang, H., Liu, H., Fu, H., and Wang, D. (2022). Forsythoside A Mitigates Alzheimer's-like Pathology by Inhibiting Ferroptosis-mediated Neuroinflammation via Nrf2/GPX4 Axis Activation. Int. J. Biol. Sci. *18*, 2075–2090. https://doi.org/10.7150/ijbs.69714.
43. Tong, J., Lan, X.T., Zhang, Z., Liu, Y., Sun, D.Y., Wang, X.J., Ou-Yang, S.X., Zhuang, C.L., Shen, F.M., Wang, P., and Li, D.J. (2023). Ferroptosis inhibitor liproxstatin-1 alleviates metabolic dysfunction-associated fatty liver disease in mice: potential involvement of PANoptosis. Acta Pharmacol. Sin. *44*, 1014–1028. https://doi.org/10.1038/s41401-022-01010-5.
44. Lin, C.P., Huang, P.H., Chen, C.Y., Tzeng, I.S., Wu, M.Y., Chen, J.S., Chen, J.W., and Lin, S.J. (2023). Tributyrin Intake Attenuates Angiotensin II-Induced Abdominal Aortic Aneurysm in LDLR(-/-) Mice. Int. J. Mol. Sci. *24*, 8008. https://doi.org/10.3390/ijms24098008.
45. Lei, C., Kan, H., Xian, X., Chen, W., Xiang, W., Song, X., Wu, J., Yang, D., and Zheng, Y. (2023). FAM3A reshapes VSMC fate specification in abdominal aortic aneurysm by regulating KLF4 ubiquitination. Nat. Commun. *14*, 5360. https://doi.org/10.1038/s41467-023-41177-x.
46. Tanasković, I., Mladenović-Mihailović, A., Usaj-Knezević, S., Stanković, V., Aleksić, A., Kastratović, T., Aleksić, A., Lazić, Z., Mladenović-Bogdanović, Z., Zivanović, A., et al. (2010). [Histochemical and immunohistochemical analysis of ruptured atherosclerotic abdominal aortic aneurysm wall]. Vojnosanit. Pregl. *67*, 959–964. https://doi.org/10.2298/vsp1012959t.
47. Atkinson, G., Bianco, R., Di Gregoli, K., and Johnson, J.L. (2023). The contribution of matrix metalloproteinases and their inhibitors to the development, progression, and rupture of abdominal aortic aneurysms. Front. Cardiovasc. Med. *10*, 1248561. https://doi.org/10.3389/fcvm.2023.1248561.
48. Rabkin, S.W. (2017). The Role Matrix Metalloproteinases in the Production of Aortic Aneurysm. Prog. Mol. Biol. Transl. Sci. *147*, 239–265. https://doi.org/10.1016/bs.pmbts.2017.02.002.
49. Frismantiene, A., Philippova, M., Erne, P., and Resink, T.J. (2018). Smooth muscle cell-driven vascular diseases and molecular mechanisms of VSMC plasticity. Cell. Signal. *52*, 48–64. https://doi.org/10.1016/j.cellsig.2018.08.019.
50. Zheng, J.P., He, X., Liu, F., Yin, S., Wu, S., Yang, M., Zhao, J., Dai, X., Jiang, H., Yu, L., et al. (2020). YY1 directly interacts with myocardin to repress the triad myocardin/SRF/CArG box-mediated smooth muscle gene transcription during smooth muscle phenotypic modulation. Sci. Rep. *10*, 21781. https://doi.org/10.1038/s41598-020-78544-3.

STAR★METHODS

KEY RESOURCES TABLE

REAGENT or RESOURCE	SOURCE	IDENTIFIER
Antibodies		
GPX4 Antibody	Abclonal	Cat # A1933; RRID: AB_2763960
FTH1 Antibody	Proteintech	Cat # 83428-1-RR; RRID: AB_3671075
SLC7A11 Antibody	Proteintech	Cat # 26864-1-AP; RRID: AB_2880661
MMP2 Antibody	Abcam	Cat # Ab86607; RRID: AB_10672798
MMP9 Antibody	Abcam	Cat # Ab76003; RRID: AB_1310463
OPN Antibody	Proteintech	Cat # 22952-1-AP; RRID: AB_2783651
α-SMA Antibody	Affinity	Cat # BF9212; RRID: AB_2839428
Nrf2 Antibody	Proteintech	Cat # 16396-1-AP; RRID: AB_2782956
HO-1 Antibody	Proteintech	Cat # 10701-1-AP; RRID: AB_2118685
IL-1β Antibody	Cell signaling technology	Cat # 31202; RRID: AB_2799001
IL-6 Antibody	Abclonal	Cat # A0286; RRID: AB_2757098
TNF-α Antibody	Abclonal	Cat # A0277; RRID: AB_2757090
GAPDH Antibody	Proteintech	Cat # 60004-1-Ig; RRID: AB_2107436
Chemicals, peptides, and recombinant proteins		
(Phenylthio)acetic acid	Aladdin Biochemical Technology	Cat #P101811
Selenomethionine	Aladdin Biochemical Technology	Cat #S130045
Experimental models: Cell lines		
Vascular smooth muscle cells	GuangZhou Jennio Biotech Co.,Ltd.	Cat # JNO-M0177
Experimental models: Organisms/strains		
C57BL/6Jmice	Guangzhou Ruge Biotechnology Co., Ltd.	NA
Software and algorithms		
GraphPadPrism	GraphPadSoftware,LLC	V9
Origin	OriginLab	V2021
Fiji ImageJsoftware	ImageJ.org	V1.53

EXPERIMENTAL MODEL AND STUDY PARTICIPANT

Cell culture

The VSMCs were purchased from GuangZhou Jennio Biotech Co.,Ltd. (Guangzhou, China) and cultured in DMEM/F12 media (Gibco) supplemented with 10% FBS, 1% penicillin, and streptomycin.

Animal experiment

Twenty-four 6-week-old male C57 mice were purchased from Guangzhou Ruge Biotechnology Co., Ltd., and randomly divided into 4 groups: control, AAA, PDPs and PDPs-Se ($n = 6$). After anesthesia, a midline incision was made in the abdomen to expose the auxiliary arteries. A gauze soaked in a calcium chloride solution was placed on the outer membrane of the abdominal aorta and incubated for 10 min. The abdominal cavity was then cleaned with PBS and closed. After 4 weeks, the PDPs group and PDPs-Se group were injected with 100 μL of PDPs and PDPs-Se (15 μg/mL) intravenously, while the control group and AAA groups received the same amount of normal saline, respectively. The animal experiments were approved by the Animal Ethics Committee of Guangzhou Seyotin Biotechnology Co., Ltd. (SYT2023078).

METHOD DETAILS

Preparation and characterization of dendritic polylysine-ROS -based nanoparticles

Phenylthio-modified dendritic polylysine (PDPs) was prepared as follows: first, 3.65 g of dendritic polylysine (DPs) was dissolved in 100 mL of deionized water. Subsequently, 4.2 g of EDC and 2.3 g of NHS were added to the solution and stirred at room temperature.

Subsequently, Tri-HCl buffer solution was added dropwise until the pH reached 5.5. Next, 3.36 g of (phenylthio)acetic acid was dissolved in 10 mL of ethanol and added to the solution. After 24 h of reaction, the solution was dialyzed in deionized water for over 3 days. Finally, the insoluble oily product was collected and hermetically stored in a vial at −20°C.

Phenylthio-modified dendritic polylysine nanoparticles loaded with selenomethionine (PDPs-Se) nanoparticles were further prepared by mixing 0.3 mg of selenomethionine with 10 mg of PDPs in 1 mL of deionized water. After stirring at 400 rpm for 30 min, the PDPs-Se nanoparticles were obtained by lyophilization at −80°C for 48 h.

The morphology of PDPs-Se nanoparticles was observed by field emission scanning electron microscopy (FE-SEM). The nanoparticles were collected, treated with gold spraying, and observed using FE-SEM (MERLIN, Carl Zeiss AG, Germany) at a working distance of 10 mm and an EHT of 10 kV.

The synthesized product and its raw materials (dendritic polylysine) were analyzed using a Fourier transform infrared spectrometer (FTIR, Nicolet iS5N, Thermo Fisher, USA) and H Nuclear Magnetic Resonance Spectra (1H NMR).

The chemical structure of the dendritic polylysine and synthetic product was analyzed by ultraviolet–visible spectroscopy (UV-vis). The samples were briefly dispersed in deionized water at a concentration of 10 mg/mL. After being photographed using a digital camera, the samples were transferred to a cuvette and examined using UV-vis (UV-3600i Plus, Shimadzu, Japan). ROS-responsive release of PDPs-Se were measured in different concentration of H_2O_2 solution using UV-vis. Additionally, the size distribution and zeta potential of PDPs-Se were evaluated using dynamic light scattering (DLS, LS Instruments, Switzerland).

CCK-8 assay

The toxicity of PDPs-Se nanoparticles on VSMCs was evaluated using the Cell Counting Kit-8 (CCK-8, Dojindo). The cells were seeded in a 96-well plate and induced by adding 10 μg/mL ANG-II for 24 h. After further treatment with different PDPs-Se concentrations (5, 10, 15, 20, and 25 μg/mL) for 48 h, 10 μL CCK-8 solution (Seyotin, China) was added to each well, and the absorbance at 450 nm was measured using a microplate reader.

RT-qPCR

The total RNA was extracted from freshly frozen aortic tissues using the TRIzol reagent (Invitrogen, Carlsbad, CA, USA). The extracted mRNA was reverse-transcribed into cDNA using the RevertAid First Strand cDNA Synthesis Kit (Thermo Scientific, USA). Subsequently, RT-qPCR was performed in a 20-μL reaction volume using the SYBR Green PCR premix (Seyotin, China), with GAPDH used as an internal control. The relative expression of genes was calculated using the $2^{-\Delta\Delta CT}$ method. The primer sequences are listed in Table S2.

Western blot

Following treatment with PDPs-Se for different durations, the total proteins was extracted from the tissues and cells using the RIPA lysis buffer. The protein concentration was determined using the BCA method. The samples were separated using SDS-PAGE gel and transferred onto a PVDF membrane. The membrane was blocked with 5% non-fat milk solution, washed with TBS-T 3 times, and incubated with Anti-GPX4, Anti-MMP2 (Abclonal, China) and Anti-MMP9 (Abclonal, China), followed by HRP-conjugated secondary antibodies. Finally, the protein signals were detected using the ECL detection reagent (Seyotin, China).

Immunofluorescence staining

After treatment with PDPs-Se for different durations, the cells were fixed in 4% paraformaldehyde for 15 min at room temperature and permeabilized with 0.1% Triton X-100 for 2 min. After washing with PBS 3 times, the cells were blocked in 3% normal serum blocking solution for 20 min at room temperature, followed by incubation with primary antibodies (1:100 dilution) at 4°C overnight. Subsequently, the cells were incubated with the corresponding secondary antibodies (1:200 dilution) for 60 min and DAPI solution for 10 min at 37°C. Finally, the cells were observed using a fluorescence microscope.

ELISA assay

Cellular supernatants were collected from the mice, incubated at room temperature for 90 min, and centrifuged at 3000 rpm at 4°C for 10 min. The supernatant was collected and stored at −80°C. The expression levels of SOD, MDA, and GSH proteins were measured using an ELISA kit, following the manufacturer's instructions.

Flow cytometry

The cells were inoculated into 6-well plates, treated with PDPs-Se for 24 h, washed three times with PBS, and incubated with 500 μL diluted DCFH-DA at 37°C for 20 min in a cell incubator. The probe was inverted and mixed every 3-5 min to ensure complete contact with the cells. After incubation, the cells were washed three times with a serum-free cell culture medium to remove any residual DCFH-DA. Flow cytometry (BD, USA) was used for detection.

Histological and immunofluorescence staining

After 2 weeks, blood was collected and the serum was separated. Then, the abdominal aortic tissues were isolated and fixed in 4% paraformaldehyde for 48 h. After dehydration, the tissues were embedded in paraffin. Subsequently, the tissues were cut into 4-μm

thick sections, dehydrated using an ethanol gradient solution. The pathological changes in the tissues were investigated using hematoxylin-eosin (HE) staining, TUNEL staining, and Victoria blue staining.

In vivo IVIS imaging

Fluorescent imaging of mice was performed under anesthesia for 24 h after mice ingested Cy7-labeled PDPs-Se using a living small animal multi-mode imaging system (IVIS spectrum system, PerkinElmer).

QUANTIFICATION AND STATISTICAL ANALYSIS

Statistical analyses were performed using the SPSS software (version 25.0). To compare the two groups, the t-test was used for normally distributed data. The statistical significance was defined as $p < 0.05$.